GEFR-SP 070

DATE November 1977
Revised March 1978

CONF-780203--1

TITLE: Heat Transfer with Hockey-Stick Steam Generator

AUTHORS: E. Moody, M. J. Gabler
(Atomics International)

Prepared for presentation at:

Joint U.S./Japan LMFBR Steam Generator Conference

Held in: Japan
City, State

on: February 1978
Date

This paper contains material resulting from work performed for: U.S. Department of Energy/General Electric Co.

Under Contract No. GE/AI 44501 task

Under DA

GENERAL ELECTRIC

FAST BREEDER REACTOR DEPARTMENT

SUNNYVALE, CALIFORNIA

HEAT TRANSFER WITH HOCKEY-STICK STEAM GENERATOR

by

E. Moody and M.J. Gabler (Atomics International)

ABSTRACT

The hockey-stick modular design concept is a good answer to future needs for reliable, economic LMFBR steam generators. The concept was successfully demonstrated in the 30 Mwt MSG test unit; scaled up versions are currently in fabrication for CRBRP usage, and further scaling has been accomplished for PLBR applications.

Design and performance characteristics are presented for the three generations of hockey-stick steam generators. The key features of the design are presented based on extensive analytical effort backed up by extensive ancillary test data.

The bases for and actual performance evaluations are presented with emphasis on the CRBRP design. The design effort on these units has resulted in the development of analytical techniques that are directly applicable to steam generators for any LMFBR application.

In conclusion, the hockey-stick steam generator concept has been proven to perform both thermally and hydraulically as predicted. The heat transfer characteristics are well defined, and proven analytical techniques are available as are personnel experienced in their use.

For presentation at the first joint US/Japan seminar on LMFBR steam generators, Japan, February, 1978

1.0 INTRODUCTION

The hockey-stick steam generator was developed as a part of the Company-funded Liquid Metal Fast Breeder Reactor (LMFBR) program. A 30 Mwt unit, termed the Modular Steam Generator (MSG), was fabricated and tested under AEC contract with the first steam produced July 9, 1972. The test program covered a wide envelope of operating conditions with a total steaming time of 4015 hours and sodium operating time of 9305 hours. Parametric data over a range of 1450 to 2550 psig (99-172 bars) was obtained. The thermal-hydraulic performance over the entire range was both predictable and stable.

Based largely on the MSG test success, AI was awarded a contract for design and fabrication of the steam generator units for the Clinch River Breeder Reactor Plant (CRBRP) in September 1975. CRBRP uses a recirculating superheat cycle as shown in Figure 1. The plant has three loops, each consisting of two evaporators and one superheater. The design of these units is essentially complete and fabrication is well underway.

Table 1 presents typical CRBRP steam generator performance characteristics comparison to that of the MSG design. It should be noted that the MSG always operated with a small degree of superheat, thus direct comparison to the CRBRP evaporator is not possible. Similarly, direct superheater comparison cannot be made since the MSG test did not have a saturated steam source. However, the MSG tests essentially envelope the CRBRP operational regime.

Table 1 also presents PLBR design data for units applicable to the three cycles currently considered. For many reasons, AI strongly favors the Benson (once-through superheat) cycle. However, the basic hockey-stick design concept is applicable regardless of cycle.

It is of interest to note from Table 1 that there is a constant multiplier of ∿3 in the evolution from MSG to PLBR. This is shown graphically in Figure 2. The transition from the MSG to CRBRP was accomplished primarily by increasing the number of tubes and maintaining the length. The transition to PLBR required an increase in both length and number of tubes. In all units, the tube dimensions and pitch have been held essentially constant with the exception of the saturated cycle PLBR evaporator.

Table 2 presents typical design characteristics of the units. It is seen that the CRBRP evaporator and superheater units are the same size. Optimally, the evaporator could be ∿3 ft shorter than the superheater. From a systematic standpoint, however, interchangeability appeared to be desirable and this factor swayed the final selection.

It is seen that the peak heat flux has been reduced from MSG to CRBRP to PLBR. This is desirable from a structural fatigue standpoint and is of primary concern in the DNB zone. Note that for the PLBR saturated cycle, this peak heat flux is reduced to reasonable levels only by using protective outer tubes.

Note also that the PLBR saturated cycle uses much larger tubes. This developed from studies showing that at low pressures larger tubes are more economical. The tube wall ΔT has also been decreased for structural purposes. That shown for the saturated cycle is across both the steam and protector tubes.

The data presented has been based on extensive testing and analyses. The subsequent sections of this paper deal with the more detailed aspects of the design, test, and analyses used to develop these performance characteristics.

2.0 HOCKEY-STICK STEAM GENERATOR FEATURES

Basically the hockey-stick steam generator is a simple, straight shell and tube, counter flow heat exchanger with an offset leg which provides flexibility to accommodate tube to shell and tube to tube differential thermal expansion. The unit is mounted vertically with the sodium flowing downward through the shell and the water-steam flowing upward through the tubes. This arrangement provides excellent natural convection flow for decay heat removal purposes.

Figure 3 shows the CRBRP units which serve either as evaporators or superheaters. Dual sodium outlet nozzles are provided for splitting the superheater flow to the two evaporator modules. In evaporator service, one outlet nozzle remains capped.

From a thermal standpoint, the design must provide: (1) stable, reliable performance over a wide range - normally 40 to 110%, (2) thermal protection of structural components over a wide range of transient conditions, and (3) performance at minimum cost. The following sections address these specific points.

2.1 Performance Features

By necessity, the sodium must be introduced through piping at right angles to the tube bundle. To most effectively utilize the available heat transfer surface, this flow must be turned and simultaneously distributed evenly across the bundle. As shown in Figure 3, this is accomplished by introducing the nozzle flow into an annulus around the bundle which turns the flow upward and distributes it evenly around the annulus. This even distribution is accomplished by eccentric flow straightener rings.

The flow is then turned inward through six flow windows. A double tube spacer is provided above the flow window to minimize circulation into the stagnant hockey stick region. A disc-donut arrangement was used on the MSG; however, concern over sodium-water reaction effects led to the double spacer arrangement which has a lower resistance. As a result, there is some recirculation above the double spacer which provides additional margin on heat transfer area and does not significantly affect the usefulness of the stagnant region in transient accommodation.

The tube bundle is arranged on a triangular pitch and is enclosed in a shroud which fits as closely as practical to the outermost tubes. However, this arrangement results in open areas around the periphery of the bundle which can lead to significant bypass flow. In order to counteract this effect, the tube spacers (required for structural support) are designed as drilled plates with sodium flow holes between tubes but without openings in the bypass area. This approach forces the bypass flow back into the bundle at each spacer thereby minimizing the bypass effect.

In the area just below the windows, the tube spacers are placed closer together than required from a structural standpoint (approximately half spacing). This arrangement provides an impedance to axial flow which is greater than the tube bundle cross flow impedance. As a result, even flow distribution across the bundle is attained in a very short axial distance, thus minimizing the less efficient cross flow heat transfer area. The flow has now completed its 90^{o} turn and flows uniformly downward through the bundle.

At the exit area of the tube bundle, spacers and windows are arranged in the reverse order to accomplish the transition from vertical tube bundle flow to horizontal nozzle flow. Again, there is some recirculation flow in the stagnant sodium between the lower windows and tubesheet having essentially the same effect as the upper recirculation.

As shown in Figure 3, the active tube length is taken conservatively as the center-to-center dimension between windows. Sections 4.0 through 6.0 of this paper treat the hydraulics and performance of the design in more detail.

2.2 Thermal Protection Features

During most transients, the sodium and water-steam temperatures follow each other very closely since plant control systems regulate flows to match required heat removal. Additionally, the thin walled tubes have small capacitances and respond rapidly to temperature changes in either fluid.

The massive shell, support, header, and tubesheet sections required from pressure and seismic consideration, on the other hand, respond quite slowly to fluid temperature changes. As a result, transients can engender large thermal gradients across these thick sections and, unless protection is provided, unacceptable thermal stresses can develop. The primary concerns are in the area of creep and fatigue damage over a 30 (CRBRP) and 40 (PLBR) year life. PLBR transients are much less severe than CRBRP, therefore design simplification is anticipated.

Figure 4 shows an exploded view of the CRBRP steam generator components. The primary means of protecting the massive pressure boundary components is by placing steel and stagnant sodium between them and the flowing sodium.

In the nozzles, this is accomplished with pinned liners which contain the flow and separate it from the nozzle proper. This liner slip fits into the header liner which protects the header from the annular flow toward the windows. Seal rings are provided to prevent flow into the annulus between the shroud and shell.

The shroud performs the function of containing tube bundle flow and providing thermal separation from the shell. In addition, the annulus sodium gap and shroud protect the shell from damage by the flame front of a sodium-water reaction. The shroud was continued fully into the elbow region for the CRBRP units whereas it ended half way into the elbow in the MSG. The primary reason for this was the severity of the CRBRP transients.

Finally, tubesheet protection is provided by thermal baffles placed at the face of each tubesheet. These baffles provide thermal capacitance to absorb temperature gradients before they can reach structural members as do the liners in the nozzle and shell regions.

This aspect of thermal protection of structural members required a massive analytical effort for the CRBRP final design. In order to accomplish this task, a sophisticated thermal/stress analysis system using extremely detailed models was developed. The reader is directed to Reference 1 for details of this system.

2.3 Economic Features

The primary parameters which affect steam generator costs for a given performance requirement are tube diameter, number of tubes and tube length; any one can be the dependent variable. There are restrictions on the degree of optimization which can be attained, some of which are:

1) Tube wall DNB $\Delta(\Delta T)$ - creep-fatigue effects
2) Steam/water side velocity - erosion problems, ΔP
3) Tube length - maximum length available without welds
4) Number of welds - reliability criteria
5) Tube diameter - minimum practical for tube/tubesheet welding and fouling considerations.

Figure 5 shows the economic effect of varying tube size and number for the CRBRP. The plant requires nine installed modules plus one spare, thus the plant cost effect is ten times the unit cost effect. The cost increase effect of increasing tube diameter is primarily engendered by the corresponding increase in length, which is magnified by the effects on shell, shroud, spacers, and supports.

For a given tube diameter, an increase in the number of tubes increases tubesheet size, shell diameter and number of welds which are balanced against a length decrease. A decreased number of tubes reverses the balance resulting in an optimum point as shown.

Previous studies had determined that the 5/8-in. (15.9 mm) tube was a practical lower limit from both fabrication and fouling considerations. All configurations shown in Figure 5 are within available tube length and over the range of number of welds involved, the reliability criteria did not appear a major concern.

Further analysis was made to determine the DNB $\Delta(\Delta T)$ and the results are shown in Figure 6. Data from power plants using 2-1/4 Cr - 1 Mo tubing indicated 250 fps (76 m/sec) to be a safe limit for erosion/corrosion problems. Therefore, a conservative limit of ~200 fps (61 m/sec) was specified. The corresponding $\Delta(\Delta T)$ of 58°F (32°C) was deemed acceptable from a structural analysis and the 757 5/8-in. (15.9 mm) O.D. tube configuration became the reference design. It can be seen from Figure 5 that the selected design is very close to the economic optimum.

For CRBRP, this evaluation was accomplished with hand calculations. For PLBR analyses, a computer code, SOC-II, has been developed to perform overall plant cost optimization. A section of this code is used for steam generator optimization and permits extremely accurate, detailed economic analyses within the confines of existing limits.

3.0 HEAT TRANSFER CORRELATIONS

In general, the sodium side correlations which have been, and are being, used are standard correlations from Reference 2. The primary exception to this is the use of the Graber & Rieger correlation[3] for forced convection over tubes. Since the sodium side resistance is a small fraction of the total resistance, verification of this correlation was not possible from the MSG test data. However, this correlation appears to be most complete and covers the flow and P/D ratios employed in the MSG, CRBRP and PLBR most adequately.

For calculations of thermal protection (i.e., input to stress modeling), the correlations used were the most conservative where choices exist in Reference 2. Although great care has been taken in the design to isolate stagnant sodium regions, some natural convection has been included in the thermal analysis.

The water-steam side correlations are fairly well accepted standard correlations that have been verified in the MSG with two exceptions — film boiling and the onset of DNB. The basic premise in the selection of correlations was simplicity, with a reasonable accuracy over anticipated ranges of interest. Table 3 summarizes the correlations.

The preheat portion of the evaporator is well characterized by the standard Dittus-Boelter equation. For the nucleate boiling regime, the Jens & Lottes[4] equation was selected. In this regime, the water side coefficient is so large that the selection of correlation is not critical.

In the superheat regime, the Bishop correlation[5] was found to give the best agreement to the MSG test data. This correlation is based on data at pressures ranging from 2350 to 3120 psia (160 to 220 bars). A similar correlation by Heineman, based on data from 300 to 1500 psia (20 to 100 bars), when extrapolated yields a slightly lower value. The difference is small; therefore, the larger value was selected for conservatism in transient calculations.

Departure from nucleate boiling (DNB) is characterized by a sudden drop in heat transfer resulting from a change in the heat transfer mechanism. This in turn results in a change in slope of the sodium temperature profile. The MSG test data showed this effect and also showed a more distinct change at low pressures because of the higher nucleate boiling heat flux.

The test data was compared to a number of DNB correlations found in the literature. None provided an acceptable fit; primarily because none were based on MSG geometry or test conditions. As a result, a completely new correlation[6] was developed by AI which provided the best fit to the range of MSG test data. Since the majority of AI steam generator designs are similar to the MSG, this correlation is deemed adequate. Subsequent DNB testing conducted at GE and ANL[7] tends to confirm the validity of this correlation.

Attempts to correlate the observed MSG film boiling heat transfer with normally used correlations proved unsuccessful. An equation of the form $Nu = C_1 Re^{C_2} Pr^{C_3}$ was used in the initial attempt. It was found that in using this equation, the Reynolds number power (C_2) had to be greater than one to provide reasonable data correlation. Such a value is inconsistent with any known film boiling correlation. Further evaluation of the test data indicated that there was strong evidence of a significant amount of moisture existing beyond the point where the theoretical equilibrium quality was one. The provide better correlation of the test data, an analytical technique employing thermal nonequilibrium was used.[6]

The basic model, termed Dispersed Flow Film Boiling, included the effects of thermal nonequilibrium and gave an accurate description of the physical flow and heat transfer processes occurring. Three different heat transfer processes were included. Heat transfer between the vapor and wall, the vapor and droplets, and the water droplets and the wall.

It was found that the dispersed flow film boiling model, with a suitably adjusted initial droplet size correlation, provided an accurate fit to the test data over the complete range of pressures and mass flows. However, due to the complexity of the model and the questionability of its application to the higher mass flow rate at CRBRP conditions, it was decided that a best fit of a modified Tong correlation to the AI-MSG data would be made.

A large uncertainty was attached to this correlation, since it yielded a relatively poor fit to the AI-MSG data in the CRBRP pressure range. Therefore, the application of this correlation to sizing the CRBRP evaporator module led to large uncertainty margins. In a subsequent effort to minimize the size of the steam generator, the film boiling correlation for use on CRBRP was re-evaluated.

A survey of the literature showed that the Bishop et al film boiling correlation[5] was applicable to the CRBRP steam conditions. This correlation is an equilibrium correlation as is the Tong correlation, and is relatively easy to model compared to the complexity of the dispersed flow nonequilibrium model. A comparison of the modified Tong and the Bishop correlations was made (Figure 7) to the AI-MSG test data based on predicted heat transfer length. It should be noted that the Tong correlation used in the comparison had been modified to match the test data as well as possible before the comparison was made.

It is apparent that a flattening trend occurs to the curves in Figure 7 at higher mass flow rates. This could be anticipated since the correlations used for film boiling in each case is of the equilibrium type, and the high end of the test data water flow rates tend toward equilibrium conditions. The equilibrium correlations should be good at water mass flows high enough to be in the equilibrium zone. The Bishop correlation tends to approach the proper heat transfer coefficient at the high end of the test flow rates. The modified Tong correlation tends to underpredict the proper heat transfer coefficient at equilibrium conditions by $\sim$50%.

The CRBRP steam generator mass flow rate is significantly higher than the test data range, and will operate with equilibrium film boiling. Note that the CRBRP mass flow rate is constant over the 40 to 100% power operating range since a constant speed recirculation pump is used. Also, film boiling in CRBRP is in a low range of steam quality (25 to 50%), where significant nonequilibrium effects would not be anticipated even at the lower mass flow rates of the AI-MSG test conditions. This conclusion is based on the fact that the Bishop correlation was shown to match the AI-MSG film boiling heat transfer rates well for equilibrium qualities of <50%.

Based on these two factors, (1) the CRBRP steam generator mass flow rate is high, and (2) the quality of steam in the film boiling region low, equilibrium film boiling will persist in the CRBRP and the Bishop correlation is believed to be applicable.

4.0 SODIUM HYDRAULICS

Sodium side pressure drop for the CRBRP evaporator and superheater modules is currently based upon results of the Hydraulic Test Model (HTM). Prior predictions had been based upon the MSG hydraulic test. Since the flow paths through the MSG and the CRBRP units are similar, loss factors experimentally determined for the MSG were applied to make a pressure drop prediction prior to the CRBRP hydraulic test. The pretest prediction was only 5% higher than the actual measured pressure drop. Therefore, the validity of using standard hydraulic correlations was confirmed by test.

Sodium flow distribution for the CRBRP steam generator modules has been determined experimentally.[8] Since the CRBRP steam generator design provides for individual tube to tube thermal expansion, uniform flow distribution does not have the same degree of importance as in a straight shell and tube unit, where a small tube to tube temperature differential can cause the tubes to buckle. However, the CRBRP design still requires uniformity of flow for thermal performance, as well as to minimize radial and circumferential thermal gradients. The purpose of the hydraulic test was twofold: first to determine vibration characteristics, and second to measure shell-side flow distribution and pressure loss. The test was performed by AI under contract to GE-FBRD. A carbon steel model (the HTM) was designed, fabricated, and tested by AI from June 1974 to June 1976. The model was full-size, identical to the prototype steam generator in internal configuration except that its active length was shortened from 46 ft (14 m) to 25 ft (7.6 m). The test was performed in a closed loop water test facility at the Rocketdyne Division of Rockwell International. This facility is designed for water flow testing of components up to 32,000 gpm (121,000 ℓ/min) The HTM was tested at flow rates up to 30,000 gpm (114,000 ℓ/min) for the flow distribution tests.

Flow velocities were measured throughout the unit to determine flow distribution. Instrument ports were provided at 30 axial locations, with capability to survey across the diameter of the unit every 60°. Two and three dimensional pitot tubes were used with water manometers to determine local velocities. An error analysis was performed to determine the accuracy of the data taking process and equipment. It was concluded that the method used was capable of ±5% resolution of the actual velocity distribution.

Flow distribution test results are presented in Reference 8. Velocity measurements in the inlet flow annulus indicate that the local flow rate at 180° from the inlet was about three times the flow rate in line with the inlet. However, the maldistribution attenuated to about 5% nonuniformity in the bundle at the inlet windows and became uniform 4 ft (1.2 m) below the windows. Flow distribution through the module is shown in Figure 8.

Based upon the results of the hydraulic test, a design modification of the inlet flow straightener rings was made to promote uniform flow distribution in the annulus. This will eliminate any possibly deleterious effects of such maldistribution, such as locally high cross flow velocities in the inlet window area. As the flow distribution was good in the tube bundle initially, the inlet annulus design change will not significantly improve flow distribution there.

5.0 WATER-STEAM HYDRAULICS

Water-steam pressure drop is calculated for the steam generator based upon frictional pressure loss, pressure loss due to momentum change, and the pressure loss due to elevation change. Standard hydraulic correlations are used to calculate these losses. These correlations have been used to match steam side pressure drop data from the AI-MSG tests.[6] The test conditions generally covered the CRBRP operating conditions. The correlations matched the test data within a ±15% error band.

Water side stability was investigated for the evaporator modules for both static and dynamic instabilities. Static instability occurs when a small flow disturbance produces a different steady state operating condition (excursive flow) or periodic flow behavior. Dynamic instability occurs when inertia and other feedback effects play an essential part in the process.

Static flow instability was investigated for both excursive flow and periodic flow behavior. Excursive flow (Ledinegg instability) is relatively simple to predict. The overall pressure drop is made up of contributions from the inlet losses, orifice, hydrostatic head, frictional head, momentum head and exit losses. The pressure drop (Δp) can be shown to be a cubic in terms of flow[9] so that for a particular range of Δp, it may be possible to sustain three different flows. Operation in this range results in a sudden drop in flow rate. The onset of such an instability is predicted when the slope of the Δp/flow rate (W) curve becomes smaller than the slope of the supply $\Delta p/W$ curve (the pump characteristic). Conservatively, this may be written $\partial(\Delta p)/\partial W<0$.

The $\Delta p/W$ curves for the various operating conditions for the CRBRP steam generator module were generated using the computer program MODULE (described in Section 6.1). For this analysis, it was assumed that one evaporator module sustained feedwater flow different than the parallel module, while sodium inlet temperature, sodium flow rate, and feedwater temperature were kept fixed. Negative slopes were not observed on the $\Delta p/W$ curves, implying excursive flow behavior will not exist.

Various forms of periodic static instability have been identified, including flow pattern instability, boiling crisis instability, bumping, geysering, and chugging. The boiling crisis instability will be present since DNB does occur; however, this is not a real instability concern in the SG design sense. The other forms of instabilities are not expected to be present, based upon the configuration of the steam generator and AI-MSG testing.

Three types of dynamic instability have been evaluated — acoustic instability, pressure drop oscillations, and density wave instability. A flow is subject to acoustic instabilities when pressure waves travel through the system. In some experiments,(10) oscillations resulted from operation at the negative-sloping region of the $\Delta p/W$ curve. In other experiments,(11) conducted at pressures in the range of 3200-3500 psia (217-239 bars), the minimum heat flux for inception of the instability was 840,000 Btu/hr-ft^2 (2649 kw/m^2). With regard to the CRBRP reference system, the slope of the $\Delta p/W$ curve is positive and the maximum local heat flux (occurring during nucleate boiling) is 350,000 Btu/hr-ft^2 (1104 kw/m^2).

Pressure drop oscillations occur in systems having a compressible volume upstream of, or within, the heated section. This is a compound instability, brought about by operation on the negative sloping part of the $\Delta p/W$ curve. All reference systems are operated on the positive slope of the $\Delta p/W$ curve.

Density wave instability is the most common type of instability. A small reduction(10) of inlet flow in a heated channel increases the enthalpy rise thereby reducing the average density. For certain combinations of geometrical arrangement, operating conditions and boundary conditions, the perturbations can become self-sustained. Various parameters which affect density wave stability are summarized in Table 4. Comparison with the corresponding MSG and CRBRP parameters show inherent stability. The use of an orifice is a common method of increasing density wave stability margin.

A preliminary analysis of density wave instability was made using two different criteria, the Stenning and Veziroglu curve(13) and the Shotkin crucial boiling length.(14) Both of these evaluations show that a substantial stability margin exists for the CRBR evaporator.

A detailed analysis of density wave stability at full and part load operation and various inlet throttling conditions was made using a modified version of the DYNAM computer code.(15) DYNAM is essentially an extension of a nuclear hydrodynamic stability code to steam generator analysis. Further modifications of DYNAM were made recently at AI for purposes of the CRBRP steam generator stability analysis, including modification of heat transfer correlations to reflect the reference CRBRP steam generator correlations as well as miscellaneous improvements to DYNAM's physical modeling of the steam generator. The results of the DYNAM analysis show that the CRBRP evaporators are free from density wave instabilities. The analysis predicts the evaporator to be very stable over the 40 to 100% load range without an inlet orifice. A typical Nyquist plot produced by DYNAM is shown in Figure 9 for 100% power evaporator operation with and without an orifice. Additional stability margin is gained by the addition of the orifice, as is demonstrated in Figure 9 by the decrease in static gain with the orifice. The stability margin is also greater at part power operation.

6.0 PERFORMANCE EVALUATION

The performance of the CRBRP steam generator modules has been evaluated in great detail. The heat transfer area of the modules has been sized using an uncertainty analysis, and full power performance has been verified for the lower limits of system operating conditions. Performance evaluations have been made using the MODULE Computer Program.

6.1 Method of Analysis

The MODULE code was initially developed as a tool for evaluating the results of the AI-MSG test. The code uses a finite difference method to evaluate heat transfer characteristics of a steam generator module. The MODULE code has both design and performance options, and can evaluate any steam generator system, such as Recirculation, Benson, Sulzer, and Saturated. The design option is used to calculate the required heat transfer area of a steam generator for a required operating condition. The performance option calculates specified operating parameters for a fixed steam generator design.

The MODULE code has been verified, as required by the CRBRP steam generator specification, by comparison to a benchmark problem which was generated by GE using their own computer code, STMGEN.

6.2 Required Heat Transfer Area

The calculation of required heat transfer surface area is shown in Table 5. The required area is composed of the nominal heat transfer area (which includes allowances for corrections, plugging, and fouling) plus an additional margin for uncertainties in heat transfer characteristics.

Material orders for the CRBRP steam generator units were placed during preliminary design; the required heat transfer surface area had not yet been established. The best estimate of required heat transfer area at the time of material orders was 5700 ft^2. Subsequent analysis has shown that the required area is $\sim$7% less, which provides excess design margin. The major factor affecting the required surface area was a result of the film boiling correlation, as discussed in Section 3.0.

The MODULE code is used for the computation of the nominal heat transfer area, except for thermal corrections, which are computed separately. The thermal corrections are factors that are not included in the MODULE code, such as the effects of tube support plates, the sodium inlet and outlet annuli, heat transfer in tube surfaces outside the defined active region, water steam flow maldistribution, and sodium flow maldistribution. The overall effect of these corrections is small, ~2% of the required area.

The uncertainty margin is required to provide 95% confidence of achieving design performance. The uncertainty factors are noted in Table 5, along with the actual uncertainties assigned to each. The individual uncertainties are statistically summed to determine the uncertainty margin.

The allocation of the heat transfer surface area is shown in Figure 10. The CRBRP steam generators have large total performance margins -42.5% in the evaporator and 29.6% in the superheater.

6.3 Full Power Performance

The steam generator specification requires that full power operation be achieved with fully-fouled evaporators and superheater, applying the 95% lower limit confidence, without exceeding the specified maximum sodium flow rate and inlet temperature of 13.5 x 10^6 lbm/h, 936°F (6.1 x 10^6 kg/h, 502°C). Using the performance option of the MODULE code, the required sodium conditions for full power operation with lower limit performance of both the superheater and evaporator modules is 12.3 x 10^6 lbm/h and 936°F (5.6 x 10^6 kg/h and 502°C). Thus, the system can operate at these conditions.

It is recognized, however, that the system may be restricted in operation for some possible conditions, such as nominal or better than nominal superheater and lower limit evaporator conditions. It should be noted that this condition is a steam cycle limit and is independent of the steam generator design.

7.0 CONCLUSIONS

As a result of the MSG testing and the extensive CRBRP design and analysis effort which incorporated the results of concurrent ancillary testing, it is concluded that the hockey-stick modular concept provides a currently available, proven steam generator for LMFBR usage.

The basic design has been substantiated by an extensive (9,000 h) test of the the 30 MWt MSG. Thermal-hydraulic correlations have been validated, modified, or developed to accurately predict performance. The thermal characteristics are well defined, analytical techniques have been developed, and an adequate staff of highly experienced personnel is available.

8.0 ACKNOWLEDGEMENTS

The thermal-hydraulic design of the CRBRP steam generators is the product of efforts by many AI personnel. The authors recognize the efforts of these people, especially the following individuals: Mr. L. G. Rico, Mr. A. V. Von Arx, Dr. N. G. Galluzzo, Mr. J. M. Seda, Dr. M. P. Heisler, and Mr. K. Mori.

9.0 REFERENCES

1. "Computerized Thermal Input for Steam Generator Stress Analysis," E. Moody, R. Rico, and G. Skopp, Paper F91d presented at 4th SMIRT Conference, San Francisco (August 1977)

2. "Liquid Metal Heat Transfer," O. E. Dwyer, BNL 11936R (January 1969)

3. Atomikenergi 19, Page 23, 1972, V. H. Graber and M. Rieger

4. "Analysis of Heat Transfer Burnout, Pressure Drop and Density Data for Pressure Water," ANL 4627, 1951, W. H. Jens and P. A. Lottes

5. "Forced Convection Heat Transfer at High Pressure After the Critical Heat Flux," ASME 65 HT-31, 1965, A. A. Bishop et al

6. TR-097-330-910, "Modular Steam Generator Final Project Report," R. B. Harty (September 1974)

7. NEDM-14164, "An Evaluation of Strain Cycling Effects in the DN13 Zone of the CRBR Evaporators," P. M. Magee et al (December 1976)

8. Y. J. Lee, et al, "An Experimental Evaluation of the Flow Distribution in the CRBRP Modular Steam Generator," 77-JPGC-NE-12

9. M. Ledinegg, "Instability of Flow During Natural and Forced Circulation," USAEC Report AEC-TR-1861

10. J. A. Bourre, A. E. Bergles, L. S. Tong, "Review of Two-Phase Flow Stability," ASME 71-HT-42

11. A. A. Bishop, R. O. Sandberg, L. S. Tong, "Forced Convection Heat Transfer to Water at Near-Critical Temperature and Super-Critical Pressure," USAEC Report WCAP-2056-Part IIIB (1964)

12. J. S. Maulbetsch and P. Griffith, "A Study of System-Induced Instabilities in Forced Convection Flows with Subcooled Boiling," EURATOM Report, Proceeding Symposium on Two-Phase Flow Dynamics, pp. 405-427 (1967)

13. A. H. Stenning and T. N. Veziroglu, "A Parametric Study of Boiling Instability," ASME 64-WA/FE-28

14. L. M. Shotkin, "Stability Consideration in Two-Phase Flow," Nucl. Sci, and Eng. 28, pp. 317-324 (1967)

15. L. E. Efferding, "DYNAM, A Digital Computer Program for Study of the Dynamic Stability of Once-Through Boiling Flow with Steam Superheat," GAMD-8676 (June 26, 1968)

TABLE 1
SG PERFORMANCE CHARACTERISTICS

Parameter — Program	MSG*		CRBRP		PLBR			
Cycle	Saturated§	Benson	Recirculating		Benson	Sulzer		Saturated
Mode	EV	EV/SH	EV	SH	EV/SH	EV	SH	EV
Na Side								
Duty Unit (Mwt)	27.4	29.4	120.8	83.4	291.2	314.1	249.1	337
Flow Unit [lb/h x 10^6 (kg/h x 10^6)]	1.46(0.66)	1.21(0.55)	6.75(3.05)	13.5(6.1)	10.8(4.9)	16.2(7.35)	32.4(14.7)	14.0(6.35)
Inlet Temperature [°F (°C)]	834(446)	950(510)	866(463)	936(502)	900(482)	814(434)	900(482)	815(435)
Outlet Temperature [°F (°C)]	625(329)	678(359)	660(349)	866(463)	600(316)	600(316)	814(434)	550(288)
Pressure Drop,[psi (bars)]	9.4(0.64)	7.4(0.5)	16(1.08)	62(4.2)	10(0.68)	12(0.82)	50(3.4)	15(1.02)
H_2O Side								
Flow/Unit [lb/h x 10^6 (kg/h x 10^6)]	0.124(0.056)	0.105(0.048)	1.11(0.5)	1.11(0.5)	1.1(0.5)	1.72(0.78)	3.26(1.48)	8.7(3.95)
Inlet Temperature [°F (°C)]	468(242)	473(245)	545(285)	628(331)	470(243)	470(243)	662(350)	529(276)
Outlet Temperature [°F (°C)]	724(384)	932(500)	628(331)	905(485)	856(458)	662(350)	856(458)	549(287)
Inlet Pressure [psia (bars)]	2691(183)	2525(172)	1945(132)	1785(121)	2390(162)	2630(179)	2490(169)	1075(73.5)
Outlet Pressure [psia (bars)]	2586(176)	2434(166)	1825(124)	1535(102)	2290(156)	2570(174)	2290(156)	1040(71)
Recirculation Ratio	-	-	2:1	-	-	†	-	6:1

* Test Conditions
† 5% evaporator flow returned to condenser
§ Minimal superheat, see text
EV = Evaporator
SH = Superheater

TABLE 2

SG DESIGN CHARACTERISTICS

Parameter	Program	MSG	CRBRP		PLBR			
	Cycle	Benson	Recirculating		Benson	Sulzer		Saturated
	Mode	EV/SH	EV	SG	EV/SH	EV	SH	EV
Tube OD [in. (mm)]		0.625(15.9)	0.625(15.9)	0.625(15.9)	0.625(15.9)	0.625(15.9)	0.625(15.9)	1.50(38.1)*
Tube wall [in. (mm)]		0.109(2.77)	0.109(2.77)	0.109(2.77)	0.109(2.77)	0.109(2.77)	0.109(2.77)	0.109(2.77)
Tube pitch [in. (mm)]		1.12(28.5)	1.22(31.0)	1.22(31.0)	1.125(28.6)	1.125(28.6)	1.20(30.5)	2.34(59.4)
Number of tubes		158	757	757	2224	2434	1970	862
Active Tube Length [ft (m)]		58(17.7)	46(14.0)	46(14.0)	77(23.5)	77(23.5)	51.5(15.7)	77(23.5)
Total Tube Length [ft (m)]		69(21.0)	63(19.2)	63(19.2)	98(29.9)	98(29.9)	74(22.6)	98(29.9)
Peak Heat Flux [Btu/h-ft^{2} † (kw/m^{2})]		250,000/ 510,000 (789/1609)	350,000 (1104)	-	160,000 (504)	140,000 (442)	-	150,000§ (473)
Shell ID [in. (cm)]		22(55.9)	49(124.5)	49(124.5)	72.0 (182.9)	77.0(195.6)	82.0(208.3)	85.0(215.9)
Heat Transfer Area [ft^{2} (m^{2})]		1500(139)	5700(530)	5700(530)	28,100(2610)	30,500(2833)	16,600(1542)	26,065(2421)
Maximum Tube Wall ΔT [^{o}F (^{o}C)]		205(114)	190(106)	238(132)	130(72)	130(72)	152(84)	266(148)

* Has 41 ft (12.5 m) of 1.975/1.520 (50.2/38.6) OD/ID protective tube
† *At operating conditions that produce maximum heat flux (i.e., CRBRP evaporator at ~60% power)*
§ At inner tube
** Dependent on power level
EV = Evaporator
SH = Superheater

TABLE 3

HEAT TRANSFER CORRELATIONS

Condition	Correlation
Sodium forced convection, shell side	$Nu = \left(0.25 + 6.2 \frac{P}{D}\right) - \left(0.007 - 0.032 \frac{P}{D}\right) Pe^{\left(0.8 - 0.024 \frac{P}{D}\right)}$
H_2O preheat	$Nu = 0.023\ Re^{0.8} Pr^{0.4}$
H_2O subcooled and nucleate boiling	$h = \left(e^{P/900}/1.9\right) \left(q^{0.75}\right)$
H_2O DNB (departure from nucleate boiling)	$X_{DNB} = \frac{18.85}{\sqrt{hfg\ (\rho_g/\rho_\ell)\ G/10^6}}$
H_2O film boiling	$Nu_f = 0.0193\ Re_f^{0.8} Pr^{1.23}\ \chi$
	$+ (1 - \chi)\ (\rho_g/\rho_\ell)_b^{0.68}\ (\rho_g/\rho_\ell)_b^{0.68}$
Steam superheat	$Nu_f = 0.0073\ Re^{0.886} Pr^{0.61}$

Nomenclature

P/D = pitch/diameter ratio

Nu = Nusselt number

h = heat transfer coefficient (Btu/h-°F-ft^2)

Re = Reynolds number

Pe = Peclet number

G = mass velocity (lbm/h-ft^2)

Pr = Prandtl number

P = pressure (psia)

q = heat flux (Btu/h-ft^2)

χ = quality

ρ_g/ρ_ℓ = density ratio - vapor to liquid

hfg = latent heat of vaporization (Btu/lbm)

Subscripts

f = film

b = bulk

TABLE 4

DENSITY WAVE STABILITY PARAMETERS

Parameter	Effect and Comments	AI-MSG Value	CRBRP Evaporator
High Orifice Δp/totalΔp	Stabilizes; four reference systems stable.	0.5	0.3
High System Pressure	Stabilizing; no instabilities except performance changes were noted in AI-MSG tests.	~500-2600 psi (34-177 bar)	1500-1900 psi (102-129 bar)
Inlet Subcooling	Stability increases with decreasing subcooling until a critical value is reached, then the trend reverses.	~200 Btu/lb (~111.1 kg-cal/kg)	60-100 Btu/lb (33.3-55.6 kg-cal/kg)
Angle From Vertical	Most stable in vertical water upflow configuration.	vertical upflow	vertical upflow
Flow Inertia	High flow inertia increases stability.	0.3-0.93 x 10^6 lb/h-ft^2 (1.46-4.5 x 10^6 kg/h-m^2)	1.6 x 10^6 lb/h-ft^2 (7.8 x 10^6 kg/h-m^2)
Pump Presence	Stabilizes.	pump present	pump present
Drum	Provides additional stability margins.	no drum	drum present
Dryout	Destabilizing; however, no instabilities were observed in the AI-MSG tests.	dryout	dryout

TABLE 5

CRBRP STEAM GENERATOR MODULE HEAT TRANSFER REQUIREMENTS

Module Condition	Heat Transfer Area [ft^2 (m^2)]	
	Evaporator	Superheater
Minimum Heat Transfer Area (Clean/Clear/Smooth Tubes)	3278 (304.5)	4013 (372.8)
Thermal Corrections	99 (9.2)	37 (3.4)
Plugging and Fouling	966 (89.7)	744 (69.1)
Nominal Heat Transfer Area	4353 (404.4)	4794 (445.3)
Heat Transfer Uncertainties (95% Confidence)		
Preheat (13.7%)	50 (4.6)	- -
Nucleate Boiling (13.7%)	12 (1.1)	- -
DNB (34.6%)	396 (36.8)	- -
Film Boiling (19.2%)	247 (22.9)	- -
Superheat (13.7%)	- -	359 (33.4)
Tube Conductivity (8.2%)	149 (13.8)	161 (15.0)
Fouling (50%)	409 (38.0)	322 (29.9)
Sodium Convection (13.7%)	87 (8.1)	50 (4.6)
Statistical Sum of Uncertainties	681 (63.3)	520 (48.3)
Required Heat Transfer Area	5016 (466.0)	5314 (493.7)
Available Heat Transfer Area	5700 (529.5)	5700 (529.5)

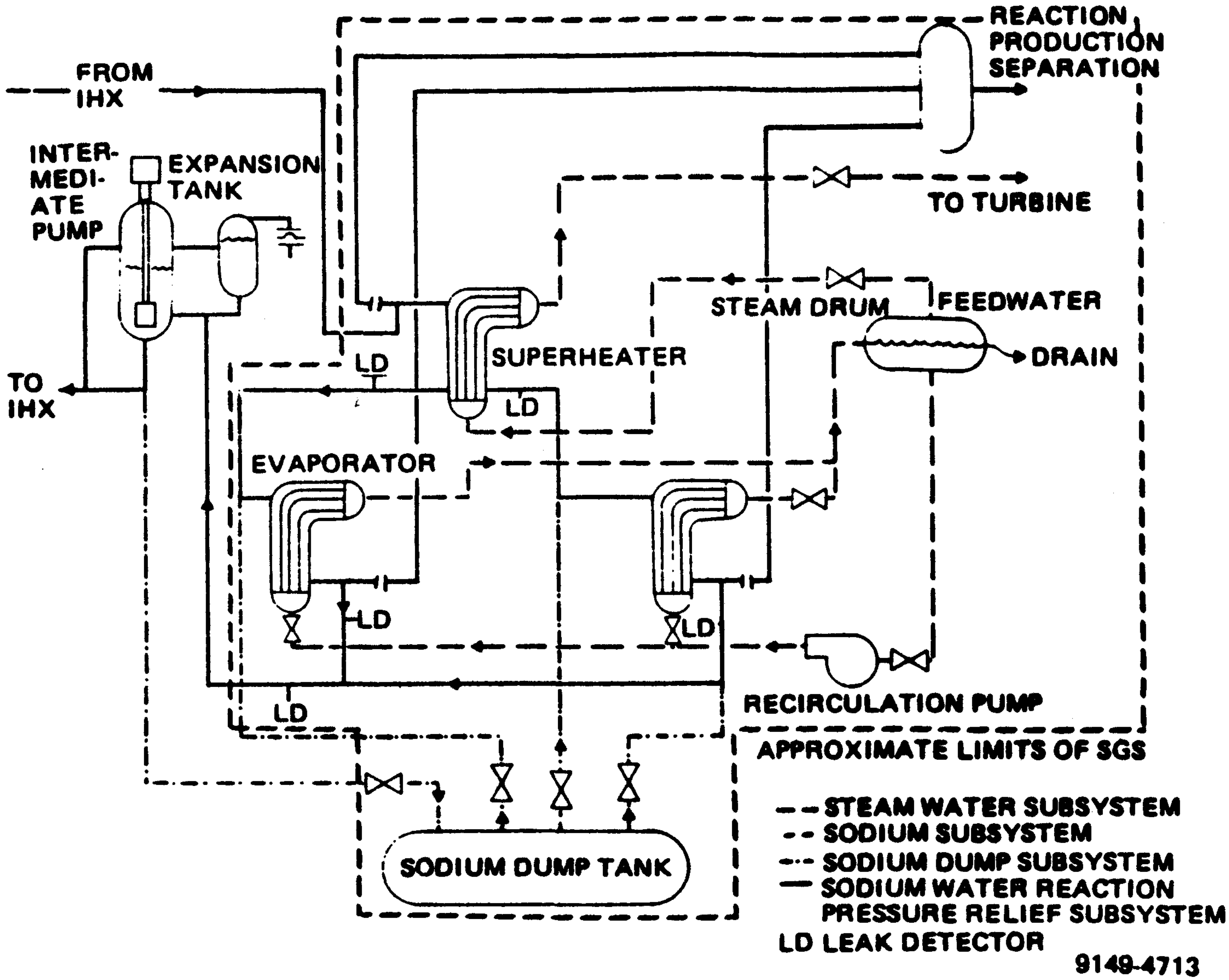

Figure 1. CRBRP Steam Generator System

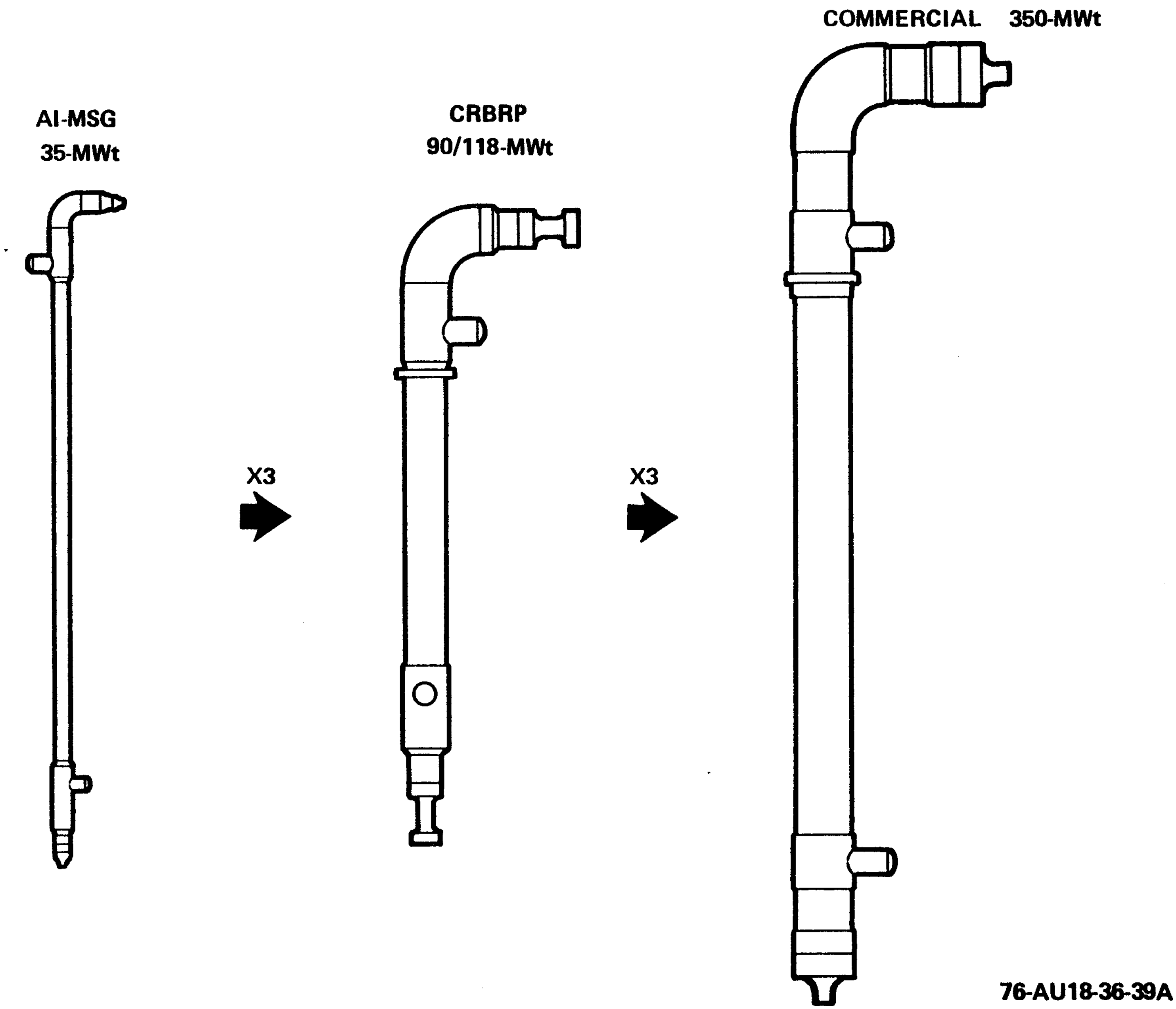

Figure 2. Evolution of Commercial Hockey-Stick Steam Generator Design

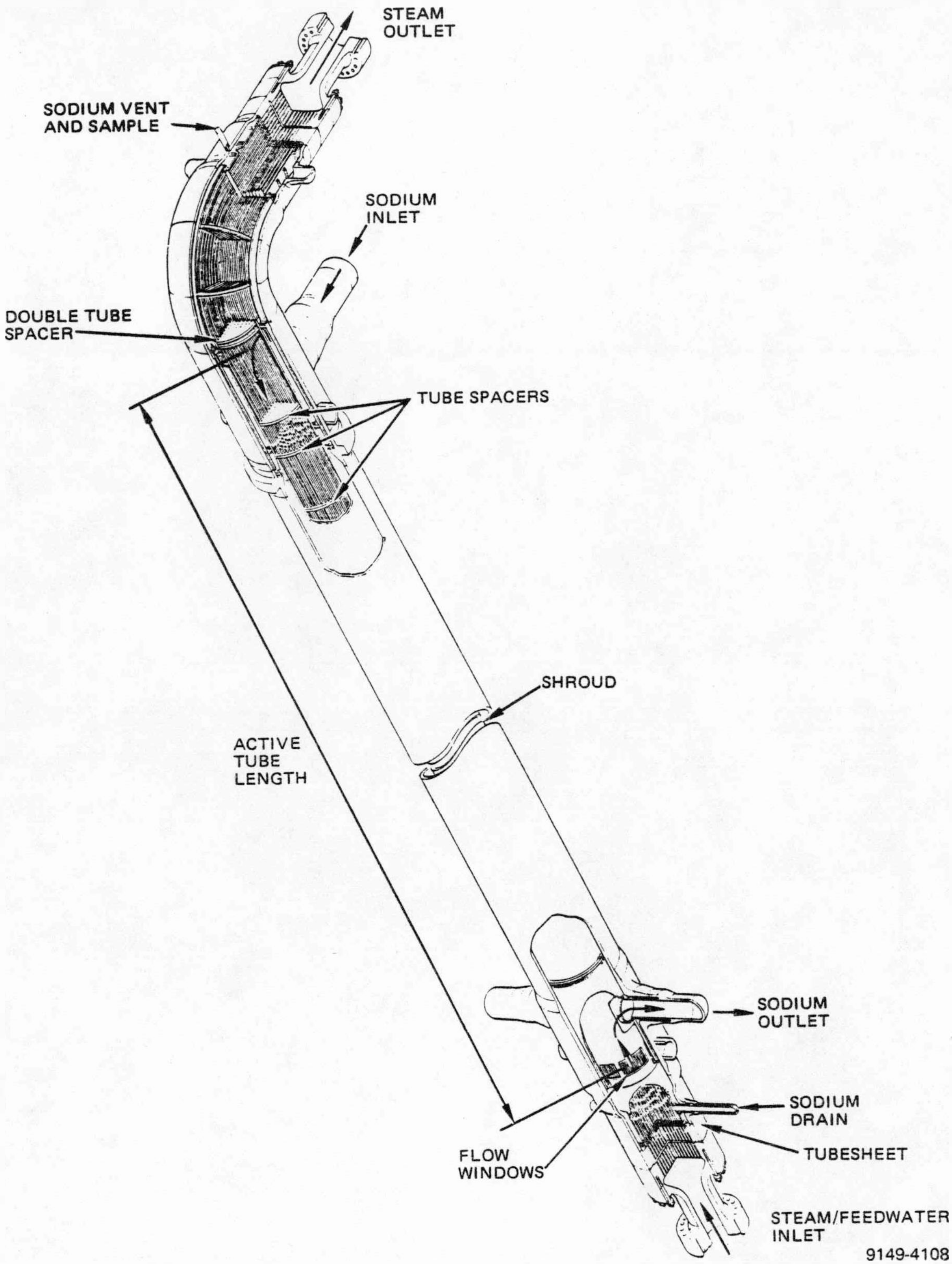

Figure 3. CRBRP Steam Generator Module

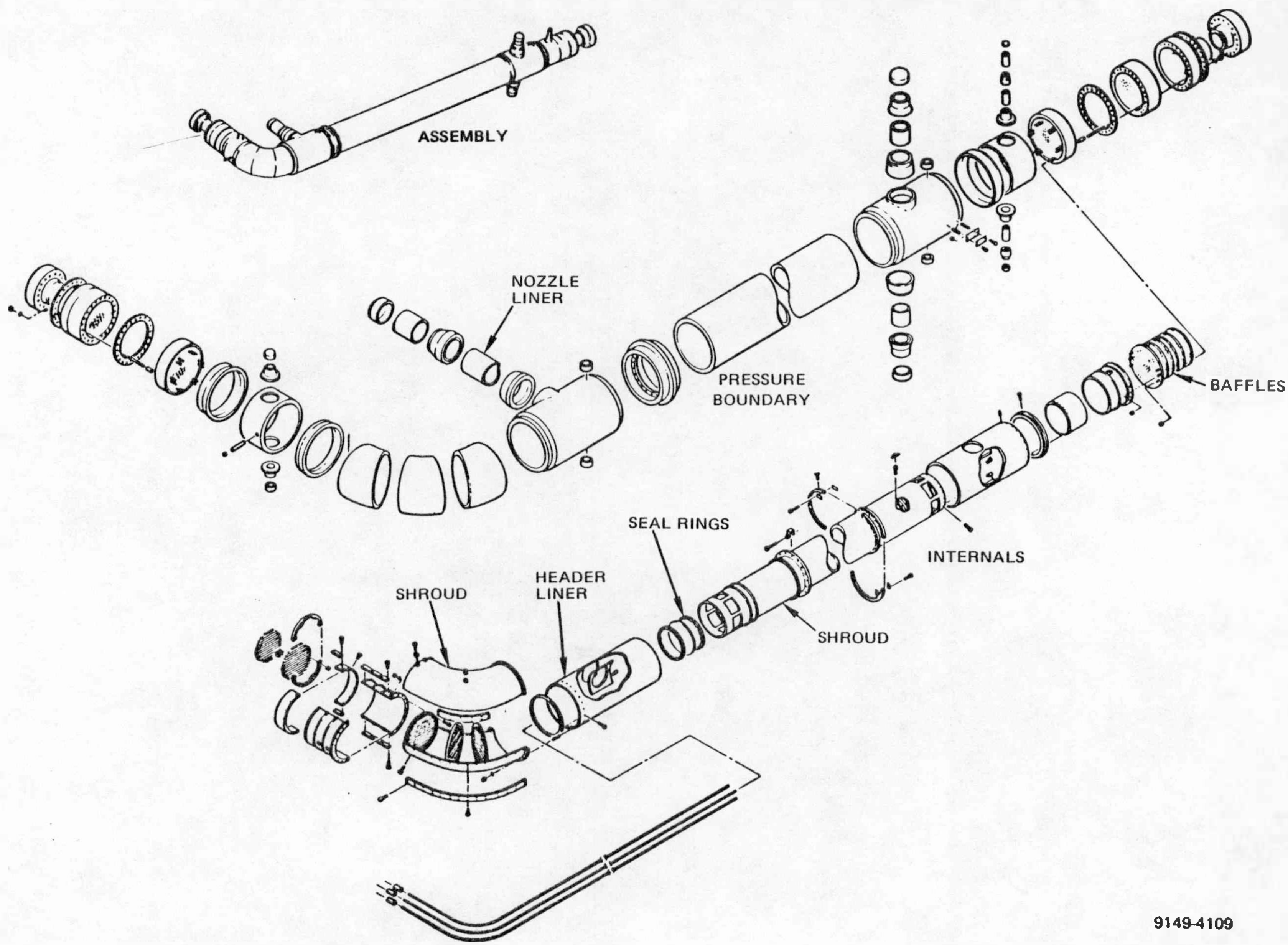

Figure 4. Steam Generator (Exploded View)

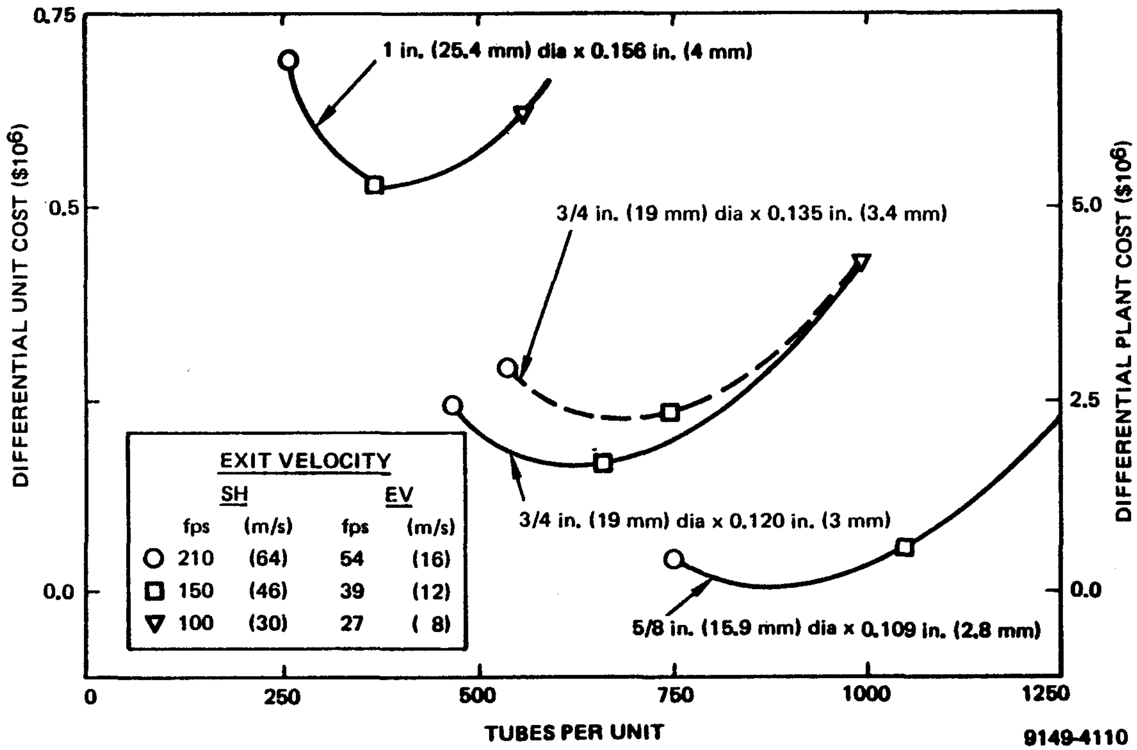

Figure 5. Economic Effect of Tubes

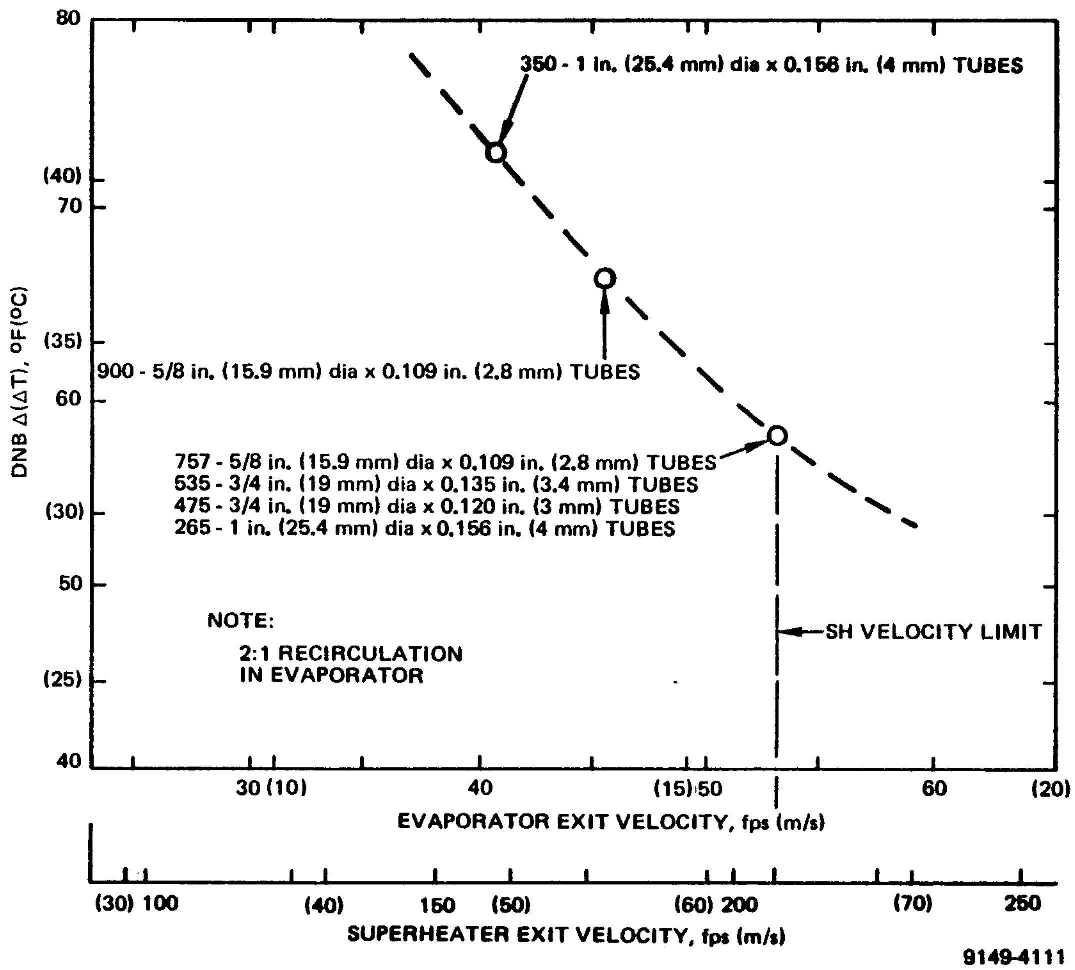

Figure 6. DNB Effect of Velocity

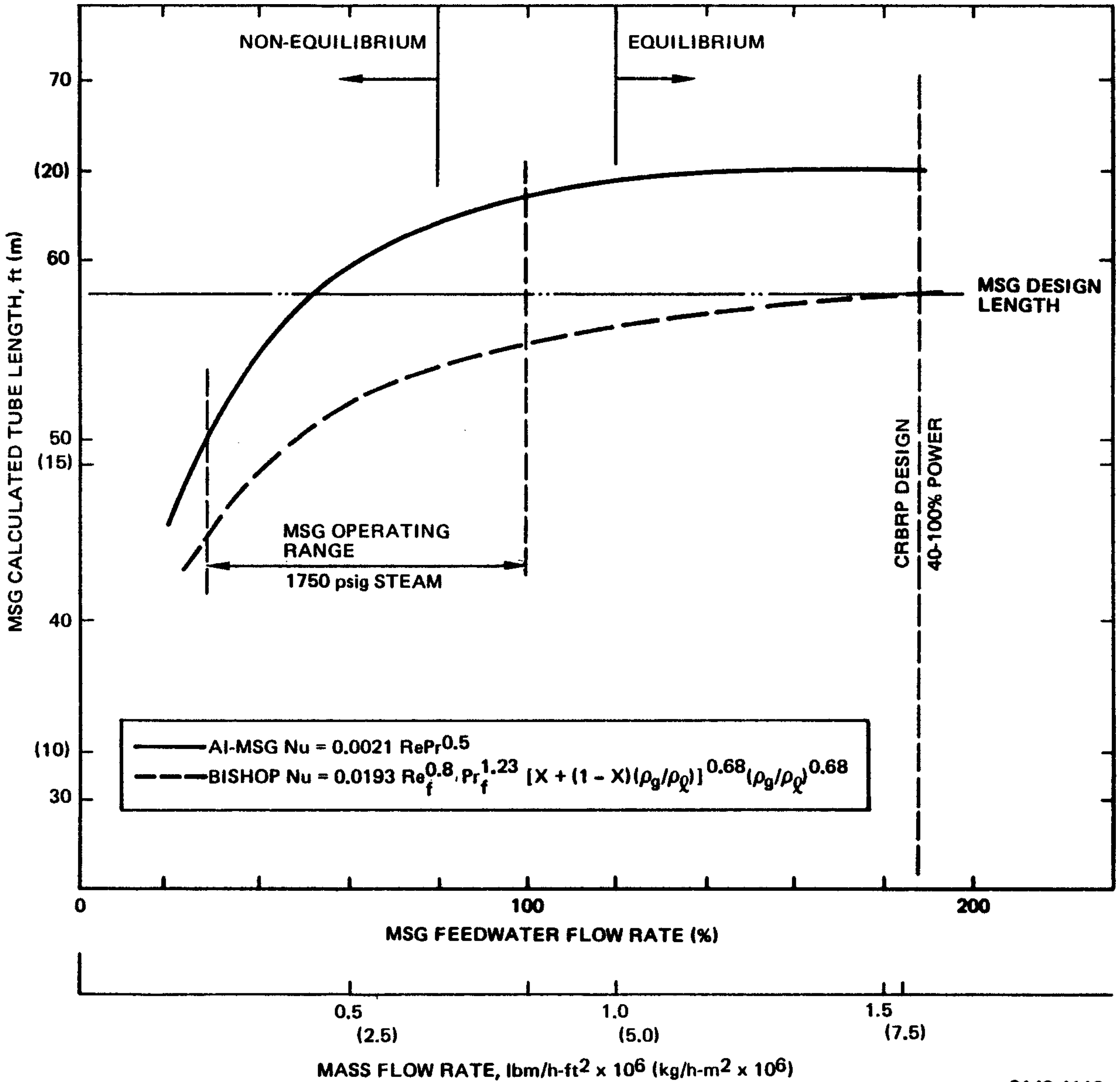

9149-4112

Figure 7. Comparison of Film Boiling Coefficients

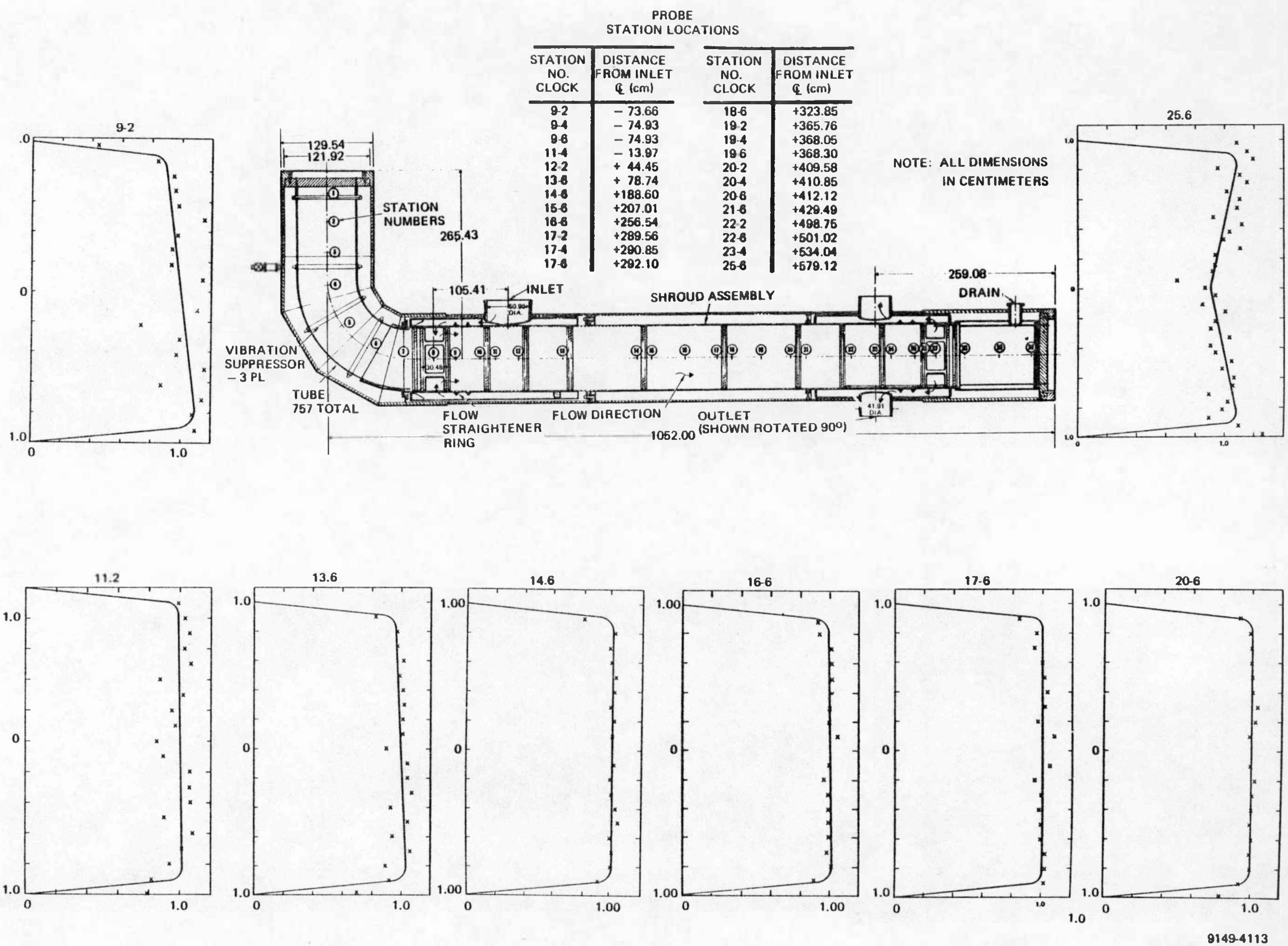

PROBE STATION LOCATIONS

STATION NO. CLOCK	DISTANCE FROM INLET ℄ (cm)	STATION NO. CLOCK	DISTANCE FROM INLET ℄ (cm)
9-2	– 73.66	18-6	+323.85
9-4	– 74.93	19-2	+365.76
9-6	– 74.93	19-4	+368.05
11-4	– 13.97	19-6	+368.30
12-2	+ 44.45	20-2	+409.58
13-6	+ 78.74	20-4	+410.85
14-6	+188.60	20-6	+412.12
15-6	+207.01	21-6	+429.49
16-6	+256.54	22-2	+498.75
17-2	+289.56	22-6	+501.02
17-4	+290.85	23-4	+534.04
17-6	+292.10	25-6	+579.12

Figure 8. CRBRP Steam Generator Hydraulic Model Flow Distribution

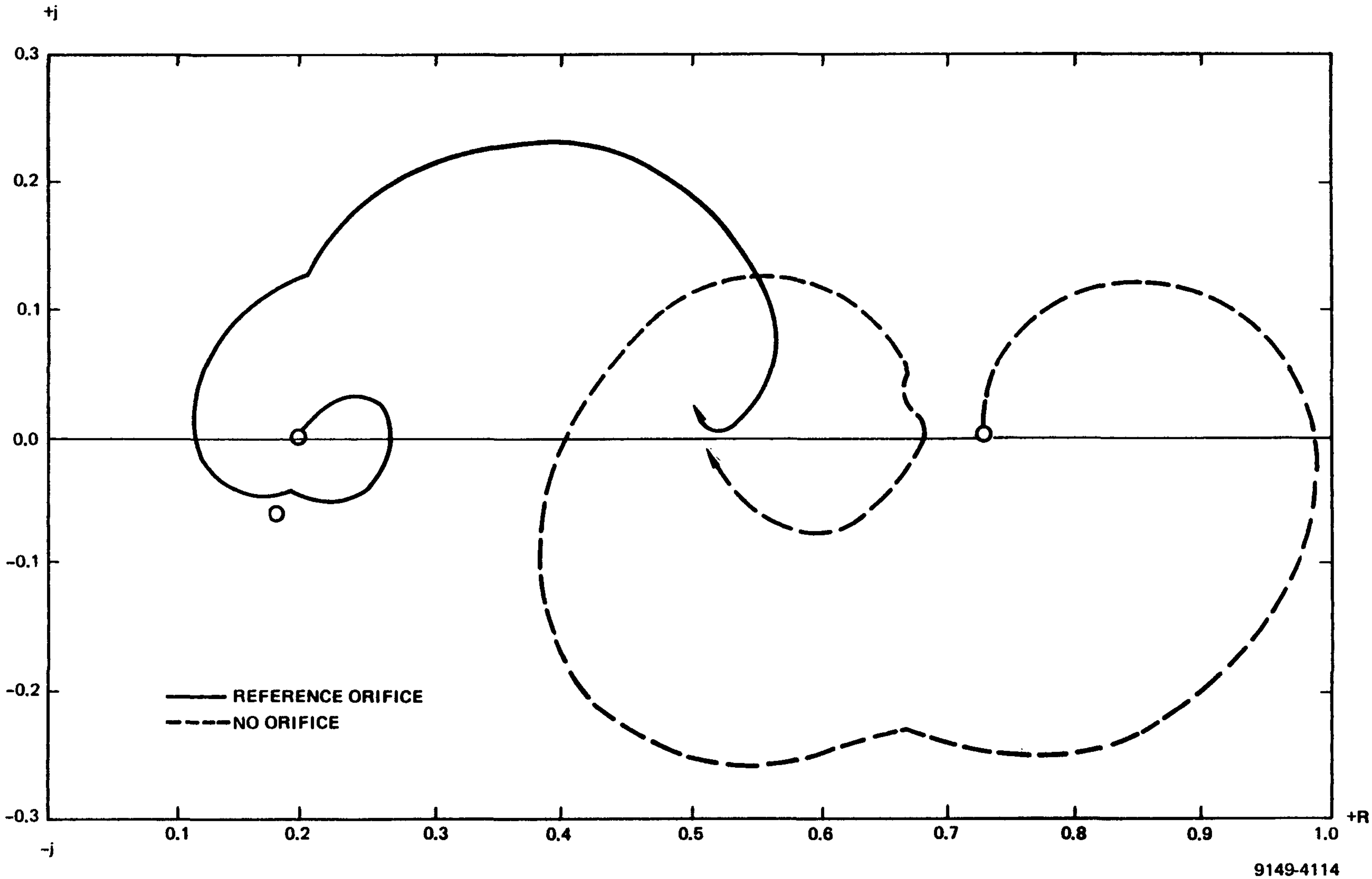

Figure 9. CRBRP Evaporator Nyquist Plot — 100% Power

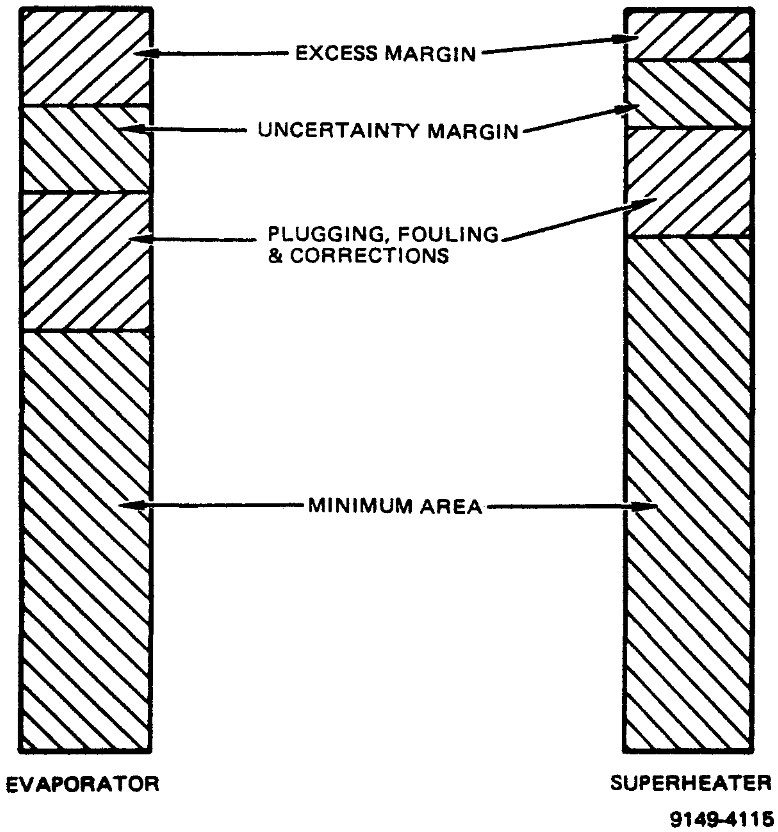

Figure 10. Allocation of CRBRP SG Surface Area